ACS Medicinal Chemistry Letters

Letter

pubs.acs.org/acsmedchemlett

GluN2A-Selective Pyridopyrimidinone Series of NMDAR Positive Allosteric Modulators with an Improved *in Vivo* Profile

Elisia Villemure,[†] Matthew Volgraf,[†] Yu Jiang,[#] Guosheng Wu,[#] Cuong Q. Ly,[†] Po-wai Yuen,[#] Aijun Lu,[#] Xifeng Luo,[#] Mingcui Liu,[#] Shun Zhang,[#] Patrick J. Lupardus,[⊥] Heidi J. A. Wallweber,[⊥] Bianca M. Liederer,[∥] Gauri Deshmukh,[∥] Emile Plise,[∥] Suzanne Tay,[∥] Tzu-Ming Wang,[‡] Jesse E. Hanson,[‡] David H. Hackos,[‡] Kimberly Scearce-Levie,[‡] Jacob B. Schwarz,[†] and Benjamin D. Sellers*[,†]

[†]Department of Discovery Chemistry, [‡]Department of Neurosciences, [§]Department of Biochemical and Cellular Pharmacology, [∥]Department of Drug Metabolism and Pharmacokinetics, and [⊥]Department of Structural Biology, Genentech, Inc., 1 DNA Way, South San Francisco, California 94080, United States

[#]Pharmaron-Beijing Co. Ltd., 6 Taihe Road, BDA, Beijing 100176, PR China

Supporting Information

ABSTRACT: The *N*-methyl-D-aspartate receptor (NMDAR) is an ionotropic glutamate receptor, gated by the endogenous coagonists glutamate and glycine, permeable to Ca^{2+} and Na^{+}. NMDAR dysfunction is associated with numerous neurological and psychiatric disorders, including schizophrenia, depression, and Alzheimer's disease. Recently, we have disclosed GNE-0723 (**1**), a GluN2A subunit-selective and brain-penetrant positive allosteric modulator (PAM) of NMDARs. This work highlights the discovery of a related pyridopyrimidinone core with distinct structure−activity relationships, despite the structural similarity to GNE-0723. GNE-5729 (**13**), a pyridopyrimidinone-based NMDAR PAM, was identified with both an improved pharmacokinetic profile and increased selectivity against AMPARs. We also include X-ray structure analysis and modeling to propose hypotheses for the activity and selectivity differences.

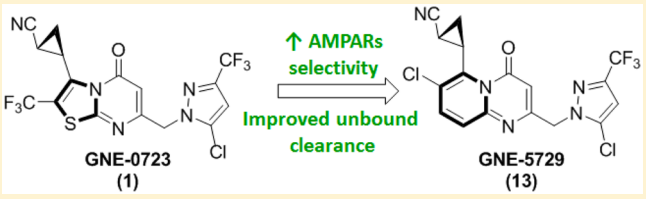

KEYWORDS: *NMDAR, PAM, AMPAR, allosteric, potentiator, selectivity, brain concentration, CNS, EPSP*

Ionotropic glutamate receptors (iGluRs) are transmembrane ion channels primarily expressed in the brain and are key regulators of neurological functions. The iGluR family consists of three congeners sharing structural similarities: the α-amino-3-hydroxy-5-methyl-4-isoxazolepropionic acid receptors (AMPARs), the kainate receptors, and the *N*-methyl-D-aspartate receptors (NMDARs).[1] NMDARs are tetramers, consisting of two GluN1 and two GluN2 subunits. In addition, NMDARs play an important role in synaptic plasticity and memory function. Structurally, NMDAR subunits include an N-terminal domain, a ligand-binding domain (LBD), and a transmembrane pore domain. NMDARs activate when two natural coagonists, glutamate and glycine, bind the LBD concurrently with membrane depolarization, which removes Mg^{2+} blockade. Once the channels are opened, Ca^{2+} and Na^{+} permeate into the cell and contribute to postsynaptic signal transmission.[2]

Isoforms of the GluN2 subunit of NMDARs, 2A, 2B, 2C, and 2D, are differentially expressed in various brain regions. In addition, it has been demonstrated that a predominant expression of GluN2B in early development shifts to GluN2A in mature synapses.[3] Literature precedents have shown that overactivation of GluN2B-containing NMDARs can lead to excitotoxicity.[4] However, little is known about the selective activation of GluN2C and GluN2D containing NMDARs.[5,6] Selective mutation or microdeletion of NMDARs containing the GluN2A subtype can recapitulate the core symptoms of schizophrenia in animal models.[7,8] NMDAR dysfunction is also implicated in a number of other neurological and psychiatric disorders, such as depression and Alzheimer's disease,[2] thus highlighting the importance of this biological target in drug discovery.

Recently, we disclosed the discovery of GNE-0723 (Table 1, compound **1**), a potent positive allosteric modulator (PAM) of GluN2A containing NMDARs.[9] The compound was identified following structure-guided improvements on a high-throughput screening hit. It is well-known that overactivation of AMPARs causes seizures.[10] Therefore, one of the main challenges of the program was to achieve selectivity for NMDARs over AMPARs ($GluA2_{Flip}$ and $GluA2_{Flop}$ isoforms),[1] a difficult problem given NMDARs and AMPARs share a PAM binding site. Even though compound **1** demonstrated good AMPAR selectivity (>200×), the pharmacokinetic profile of the molecule was not ideal, with moderate *in vivo* mouse clearance (Cl = 26 mL min^{-1} kg^{-1}) and low oral bioavailability (F= 24%). During our optimization campaign, we discovered a new pyridopyrimidinone (PP) core, replacing the previous thiazolopyrimidinone (TP) core of

Received: October 4, 2016
Accepted: October 31, 2016
Published: October 31, 2016

DOI: 10.1021/acsmedchemlett.6b00388
ACS Med. Chem. Lett. 2017, 8, 84−89

Table 1. Comparison of C′ Subsite SAR of Thiazolopyrimidinone and Pyridopyrimidinone Core

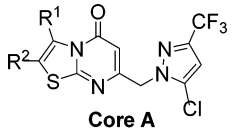

Core A

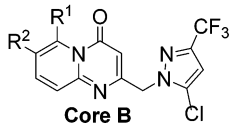

Core B

Ex	Core	R^1	R^2	EC_{50}, μM (Max potentiation, %)[a] GluN2A	$GluA2_{Flip}$	$GluA2_{Flop}$
1	A		–CF_3	0.021 (152)	9.1 (84)	5.5 (88)
2	A		–Me	0.44 (120)	37 (8)	73 (16)
3	B		–Me	2.5 (129)	(1)	(-1)
4	A		–Me	1.4 (88)	9.6 (28)	1.2 (9)
5	B		–Me	9.8 (84)	(5)	(3)
6	A		–Me	0.27 (116)	(51)	(32)
7	B		–Me	0.28 (107)	1.3 (7)	2.5 (3)
8	A		–Me	0.030 (151)	0.70 (91)	0.073 (93)
9	B		–Me	0.041 (137)	67 (66)	31 (63)

[a]NMDAR EC_{50} values were determined in the presence of EC_{30} glutamate and saturating glycine. Max potentiation (%) at 125 μM reported if no EC_{50} could be obtained, where 30% denotes the assay baseline (EC_{30} glutamate). AMPAR EC_{50} values were determined in the presence of 100 μM glutamate. Max potentiation (%) at 125 μM reported if no EC_{50} could be obtained, where 0% denotes the assay baseline due to receptor desensitization. All EC_{50} values represent geometric means of at least two determinations.

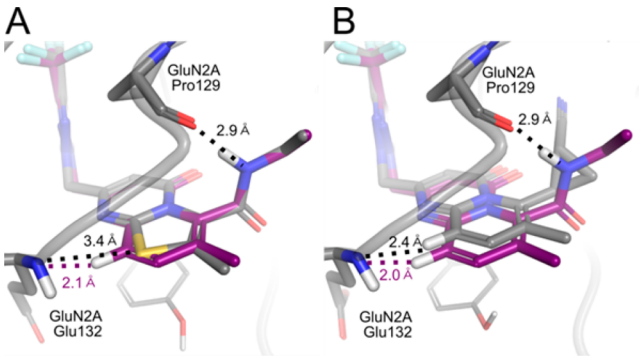

Figure 1. (A) Overlay of modeled compound **3** (purple) and GluN2A/GluN1 X-ray cocrystal structure with compound **2** (PDB ID 5TP9 gray). The amide in compound **3** may force the larger core to clash slightly with Glu132. Distances are between the Glu132 backbone nitrogen and hydrogen in **3** or sulfur in **2**. (B) Overlay of a model of compound **3** (purple) and X-ray crystal structure of compound **9** (PDB ID 5TPA, gray). The cyclopropyl nitrile in **9** may allow the larger core to shift away from Glu132. Distances are between the Glu132 backbone nitrogen and hydrogens in **3** and **9**.

compound **1**. Herein, we disclose the optimization of the PP core vectors, leading to an improved *in vivo* pharmacokinetic profile and AMPARs selectivity. We also propose structure-based hypotheses for why the structure–activity relationship and off-target selectivity of the PP core are distinct from the TP core.

In early studies of a series of GluN2A selective PAMs, we sought to explore various replacements for the thiazolopyrimidinone core. We found that few alternative cores were tolerated, suggesting that several key elements of the original

Table 2. Representative Examples of Aromatic Ring Substitution SAR

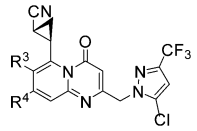

Ex	R^3	R^4	EC_{50}, μM (Max potentiation, %)[a] GluN2A	$GluA2_{Flip}$	$GluA2_{Flop}$	LM[b] H/R/M[c] (mL/min/kg)	MDR1[d] ER[e] (B:A/A:B)[f]
9	–Me	–H	0.041 (137)	67 (66)	31 (63)	7 / 43 / 62	2
10	–H	–H	0.024 (148)	0.81 (90)	0.41 (90)	6 / 5 / 32	ND[g]
11	–F	–H	0.021 (151)	3.1 (67)	0.46 (69)	3 / 13 / 31	1.5
12	–OMe	–H	0.080 (120)	(28)	(15)	7 / 46 / 56	3.2
13	–Cl	–H	0.037 (136)	45 (61)	49 (67)	2 / 34 / 34	1.6
14	–H	–Me	0.039 (144)	3.1 (86)	0.21 (83)	4 / 18 / 68	2.2
15	–H	–OMe	0.13 (140)	6.7 (51)	2.2 (67)	4 / 9 / 52	2.2
16	–H	–CF_3	0.12 (142)	27 (67)	16 (77)	10 / 23 / 32	2.1

[a]NMDAR EC_{50} max potentiation (%) and AMPAR EC_{50} values were determined as described in Table 1. [b]Liver microsome-predicted hepatic clearance. [c]H/R/M = human/rat/mouse. [d]MDCK cells transfected with human MDR1 gene. [e]Efflux ratio. [f]Basolateral-to-apical/apical-to-basolateral. [g]ND = not determined

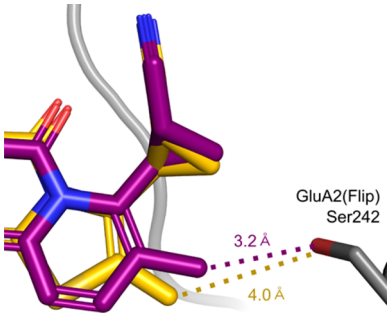

Figure 2. Overlay of modeled ligands in $GluA2_{Flip}$ (AMPAR) X-ray (PDB ID 5H8S). Compound **8** (gold) and compound **9** (purple). The core methyl group in **9** may clash more with the polar Serine242 in $GluA2_{Flip}$.

thiazolopyrimidinone core were required for potency (data not shown). One initially tolerated alternative to the TP core (Table 1, Core A) was the pyridopyrimidinone core (Table 1, Core B). The new PP core was first evaluated using a 3D shape search[11,12] of commercially available compounds[13] using the TP core-containing compound, GNE-3419 as a query (see Supporting Information Figure S-1), as described previously.[14] Moreover, the thiophene-to-phenyl bioisostere is well-precedented in the literature.[15]

We first sought to explore the structure–activity relationships (SAR) at R_1, knowing that interactions within the C′-subsite were important for potency based on previous work.[9] Lower potency was initially observed when an amide (**2** vs **3**) or a pyrimidine (**4** vs **5**) was present at R_1 when paired with the PP core. Despite the reduced potency for the PP/TP core matched pairs, very good selectivity against AMPARs was observed for those compounds. To our delight, further investigation revealed that pairing the PP core with cyclopropyl R_1 substituents (**6**–**9**)

DOI: 10.1021/acsmedchemlett.6b00388
ACS Med. Chem. Lett. 2017, 8, 84–89

Table 3. Receptor Selectivity and DMPK Properties of Compound 13

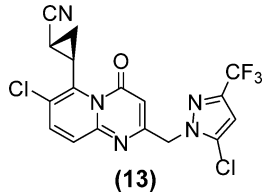

(13)

MW/LogD/TPSA		428 / 1.8 / 75	
NMDAR EC_{50} μM, (Max potentiation, %)[a] GluN2 A/B/C/D		**AMPAR EC_{50}, μM (Max potentiation, %)[b] GluA2 Flip/Flop**	
0.037 (136) / (96) / 4.7 (243) / 9.5 (140)		45 (61) / 49 (67)	
In Vitro DMPK			
LM[c] H/R/M[d] (mL/min/kg)	2 / 34 / 34	**PPB[i] (%) H/M[j]**	94.4 / 92.4
Hep[e] H/R/M[d] (mL/min/kg)	4 / 25 / 10	**Mouse Brain Binding (%)**	94.9
MDR1[f] ER[g] (B:A/A:B)[h]	1.6	**Kinetic Solubility (μM)**	43.5
Mouse PK			
IV Dosing (0.5 mg/kg)[k]		PO Dosing (5 mg/kg)[l]	
$Cl_{blood}/Cl_{blood,u}$ (mL min^{-1} kg^{-1})	10 / 132	**F (%)**	37
$t_{1/2}$ (h)	8	**$AUC_{last,u}$ (μM*h)**	0.53
V_{ss} (L/kg)	7	**$C_{max,u}$ (μM)[m]**	0.060
		$C_{brain,u}$ (μM)[n]	0.031
		$K_{p,uu}$[o]	0.67

[a,b]NMDAR EC_{50} max potentiation (%) and AMAPR EC_{50} values were determined as described in Table 1. [c]Liver microsome-predicted hepatic clearance. [d]H/R/M = human/rat/mouse. [e]In vitro stability in cryo preserved hepatocytes. [f]MDCK cells transfected with human MDR1 gene. [g]Efflux ratio. [h]Basolateral-to-apical/apical-to-basolateral. [i]Plasma protein binding. [j]H/M = human/mouse. [k]Vehicle: 10% DMSO, 10% cremophor EL in saline solution. [l]Vehicle: MCT suspension [m]Free plasma concentration at C_{max}. [n]Free brain concentration at 1 h time point. [o]$K_{p,uu} = C_{brain,u}/C_{plasma,u}$ at 1 h time point.

maintained GluN2A potency while improving AMPAR selectivity relative to earlier generation analogues. We found the best balance between GluN2A potency and selectivity against AMPARs with the cyclopropyl nitrile at R_1 (**9**). Overall, the GluN2A potency for the cyclopropyl analogues at R_1 tracked between the TP- and PP-subseries.

To help explain why the amide-PP subseries is less tolerated relative to cyclopropyl analogues, we first solved the X-ray crystal structure at 2.39 Å resolution of the TP compound **2** bound to the LBD of GluN2A/GluN1 (PDB ID 5TP9, Figure S-2, Table S-1) and then overlaid a model of the PP compound **3** (Figure 1A). We hypothesize that the hydrogen-bond between the ligand amide and GluN2A:Pro129 restricts the position of the amide in both cores. The PP core is slightly larger than the TP core and pushes a core-hydrogen orthogonally into the backbone nitrogen of Glu132 (Glu132:nitrogen to compound **3** phenyl hydrogen distance: 2.1 Å). This compares to the TP X-ray structure, which shows a ligand sulfur to Glu132 nitrogen distance of 3.4 Å. Analysis of similar H−N geometries in small-molecule crystal structures (Figure S-4) suggests 2.1 Å would result in a clash, forcing a shift in the complex and reducing potency of compound **3** compared to compound **2**. This rationale may also apply to larger R_1 substituents, which may restrict the core location, such as the pyrimidine in compound **5**.

The X-ray crystal structure of compound **9** was also solved at 2.48 Å resolution (PDB ID 5TPA, Figure S-3, Table S-1) and a core shift was observed without an amide occupying the C′ subsite (Figure 1B). When we overlaid the X-ray crystal structure of **9** with the model of compound **3**, we observed that the cyclopropyl nitrile, in contrast to the amide, does not require a specific interaction with GluN2A:Pro129, allowing the large PP core to shift away from the Glu132 backbone (2.4 Å), thus avoiding a potential steric clash with the protein. The core shift could explain the similar potencies between the PP and TP cyclopropyl nitrile compounds **8** and **9**.

We then explored substitutions at R_3 and R_4 on the six-membered pyridine ring of the PP core (Table 2). These positions are distinct from the core vectors of the five-membered

DOI: 10.1021/acsmedchemlett.6b00388
ACS Med. Chem. Lett. 2017, 8, 84−89

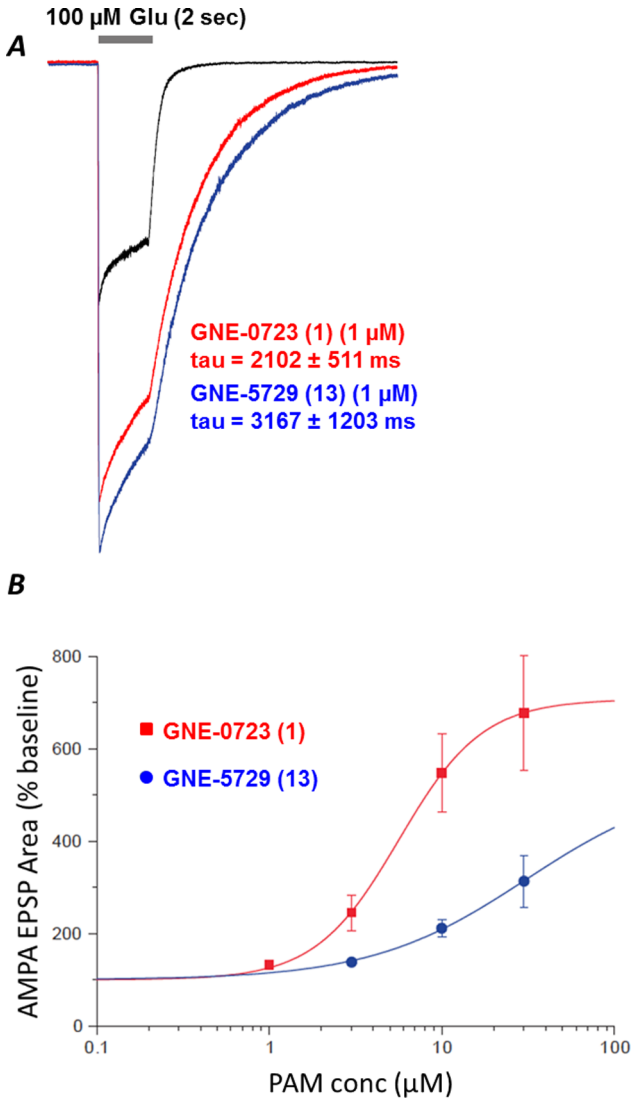

Figure 3. (A) Overlay of whole cell voltage clamp recordings comparing deactivation kinetics for GNE-0723 (**1**) in red and GNE-5729 (**13**) in blue compared to the endogenous coagonists (saturating glycine and 100 μM glutamate) in black. Deactivation "tau" is the time constant for the signal decay after glutamate is removed. (B) Dose−response curves of AMPAR excitatory postsynaptic potential (EPSP) area in brain slice field recording for GNE-0723 (**1**) (EC_{50} = 5.7 μM) and GNE-5729 (**13**) (EC_{50} > 15 μM).

thiazole-based core. We started our investigation by removing the methyl group at the R_3 position of compound **9**. Compound **10** showed a 2-fold gain in GluN2A potency at the cost of a considerable loss in AMPAR selectivity compared to compound **9**. Small R_3 substituents like fluorine (**11**) demonstrated similar GluN2A potency compared to the unsubstituted phenyl ring (**10**), but with partially improved AMPAR selectivity. The electron donating methoxy group at R_3 (**12**) possessed a unique selectivity profile, despite a 3-fold loss in potency compared to compound **10**; very low AMPAR potentiation was observed at the highest concentration tested (125 μM). However, increased efflux ratio (ER) in MDCK-MDR1 transfected cells was observed.

The chloro substituent at the R_3 position (**13**) showed good GluN2A potency and overall improved GluA2 selectivity compared to compound **9**. The chlorine also resulted in a much improved human liver microsome stability compared to all compounds tested (2 mL/min/kg). Furthermore, compound **13** had a lower efflux ratio compared to **12** (B:A/A:B = 1.6 vs 3.2), thus increasing the likelihood of achieving biologically relevant free brain concentrations *in vivo*.

Finally, we explored the substitution at the newly opened vector at R_4 enabled by the six-membered ring. Unfortunately, no improvement in GluN2A potency or AMPAR selectivity was observed with R_4 as a methyl (**14**), methoxy (**15**), or trifluoromethyl (**16**) substituent (R_3 as hydrogen).

In summary, the substitution at the R_3 position was the most beneficial for AMPAR selectivity, while maintaining good GluN2A potency. We rationalize the importance of the R_3 substituent on the PP core through modeling of compounds **8** and **9** within the previously published X-ray of TP compound GNE-3419 bound to AMPAR/$GluA2_{Flip}$ (Figure 2). We found that the methyl at R_3 of the PP core (compound **9**) is closer to the polar Serine242 in $GluA2_{Flip}$ compared to the methyl of the TP core of compound **8** (3.2 Å vs 4.0 Å). We hypothesize that compounds presenting either large or hydrophobic substituents near Serine242 may have increased selectivity over AMPAR compared to the TP analogues. Ultimately, compound **13** demonstrated the best balance between GluN2A potency and AMPAR selectivity with good overall metabolic stability across species and no evidence of efflux *in vitro*. Compound **13** was then scaled up for *in vivo* PK studies (for synthetic details, see Supporting Information).

Compound **13** (GNE-5729) possessed a good overall profile as highlighted in Table 3. Compound **13** showed favorable physicochemical properties as the molecular weight, LogD, and total polar surface area (TPSA) of the molecule were in a range to maximize the odds of success for a central nervous system drug target molecule.[16] Compound **13** had a very selective profile against various off-target ion channels with greater than a 100-fold selectivity over other NMDAR subtypes and greater than a 1000-fold selectivity over AMPAR. This is 5-fold improved selectivity against AMPAR compared to compound **1**. Compound **13** also possessed a desirable pharmacokinetic profile, including low to moderate *in vitro* clearance across species (Table 3), which translated *in vivo* (CL_{Blood} = 10 mL min^{-1} kg^{-1}) when dosed IV in mouse at 0.5 mg/kg. We found that compound **13** had a moderate bioavailability (F = 37%) while demonstrating good brain permeability (unbound brain-to-plasma concentration ratio $K_{p,uu}$ = 0.67 at 1 h) when dosed orally at 5 mg/kg. This result correlated well with the *in vitro* MDCK-MDR1 ER (B:A/A:B = 1.6) predicting low efflux, thus confirming the viability of compound **13** as potential *in vivo* tool compound.

In comparison to our previous lead molecule compound **1** (Table S-2), compound **13** showed similar brain permeability ($K_{p,uu}$ = 0.62 vs $K_{p,uu}$ = 0.67) and bioavailability (F = 24% vs F = 37%) in mouse. However, **13** demonstrated a greater free brain concentration at 1 h postdose compared to **1** ($C_{brain,u}$ = 0.031 μM vs $C_{brain,u}$ = 0.013 μM). The 3-fold *in vivo* unbound clearance improvement (Clu= 132 mL min^{-1} kg^{-1} vs Cl_u= 433 mL min^{-1} kg^{-1}) and the greater brain free fraction ($f_{u,brain}$= 0.051 vs $f_{u,brain}$= 0.014) of compound 13 resulted in higher free brain concentration. The overall pharmacokinetic profile improvement, in addition to a better kinetic solubility (kinetic solubility = 43.5 μM vs kinetic solubility = 9.3 μM), resulted in compound **13** achieving 1.6-fold free plasma concentrations above the *in vitro* EC_{50} at $C_{max,u}$. This was an important milestone toward enabling *in vivo* efficacy studies.

DOI: 10.1021/acsmedchemlett.6b00388
ACS Med. Chem. Lett. 2017, 8, 84−89

The two compounds share similar deactivation kinetics in whole cell voltage clamp recordings; both compounds are considered moderate deactivators (compound **1** tau = 2102 ms; compound **13** tau = 3164 ms) showing a 4−6-fold slower deactivation than the endogenous coagonists, glycine and glutamate (Figure 3A).[9] The tau values correlate with the compounds respective maximum potentiation values (compound **1** max potentiation = 152%; compound **13** max potentiation = 136%). Typically, a maximum potentiation greater than 100% is a good indication of a slower deactivator.[17] The improved selectivity of compound **13** over AMPAR, the main off-target liability on the program, was a considerable benefit of the new lead compound that allows for more careful evaluation of the efficacy and safety window of GluN2A PAMs without confounding AMPAR activity. To assess for potentiation of native AMPARs during physiological activation, compounds **1** and **13** were examined by excitatory postsynaptic potential (EPSP) in brain slice field recordings (Figure 3B).[18] The greater selectivity of **13** observed in the cell assay was confirmed when compound **13** showed a significantly lower potentiation of AMPARs compared to compound **1** (greater than 2.6-fold selectivity in EPSP).

A core-replacement campaign to find alternatives to the thiazolopyrimidinone core of compound **1** led to the identification of the privileged pyridopyrimidinone core, which possessed greater than 2.6-fold improved AMPAR selectivity in the biologically relevant EPSP assay. We found that the cyclopropyl nitrile at R_1 and the chloro at R_3 resulted in a balance of potency, selectivity, and brain penetration. We hypothesize that this increased selectivity originates from a unique R_3 vector situated near the Serine242 in $GluA2_{Flip}$. In retrospect, the lower unbound clearance, the improved kinetic solubility, and the increased mouse brain free fraction of compound **13** compared to compound **1** led to increased free brain exposure and EC_{50} coverage. In summary, the improved pharmacokinetic profile and AMPAR selectivity make GNE-5729 (**13**) a superior tool compound compare to GNE-0723 (**1**) for testing the efficacy and safety of GluN2A potentiation.

■ ASSOCIATED CONTENT

Supporting Information

The Supporting Information is available free of charge on the ACS Publications website at DOI: 10.1021/acsmedchemlett.6b00388.

Three-dimensional shape search identification of pyridopyrimidinone core, X-ray crystal structure of compounds **2** and **9**, histograms of Cambridge Structural Database distance statistics, receptor selectivity and DMPK properties of compound **1**, experimental procedures and characterization data for compound **13** (PDF)

■ AUTHOR INFORMATION

Corresponding Author

*E-mail: sellers.benjamin@gene.com. Tel: 1(650)467-3995. Fax: 1(650)467-5155.

Notes

The authors declare no competing financial interest.

■ ACKNOWLEDGMENTS

We thank the Genentech Analytical, DMPK, In vivo Studies and Structural Biology Groups for their contributions. Special thanks to Baiwei Lin, Kewei Xu, and Kang-Jye Chou for the analytical support.

■ ABBREVIATIONS

NMDA, *N*-methyl-D-aspartate; NMDAR, *N*-methyl-D-aspartate receptor; PAM, positive allosteric modulator; iGluR, ionotropic glutamate receptor; AMPAR, α-amino-3-hydroxy-5-methyl-4-isoxazolepropionic acid receptors; LBD, ligand binding domain; PP, pyridopyrimidinone; TP, thiazolopyrimidinone; SAR, structure−activity relationship; ER, efflux ratio; MDCK-MDR1, Madin−Darby canine kidney cells-multidrug resistance protein 1; PK, pharmacokinetic; TPSA, topological polar surface area; DMPK, drug metabolism and pharmacokinetic; LM, liver microsomes; Hep, hepatocytes; PPB, plasma protein binding; AUC, area under the curve; DMSO, dimethyl sulfoxide; MCT, methylcellulose/tween; EPSP, excitatory postsynaptic potential

■ REFERENCES

(1) Traynelis, S. F.; Wollmuth, L. P.; McBain, C. J.; Menniti, F. S.; Vance, K. M.; Ogden, K. K.; Hansen, K. B.; Yuan, H.; Myers, S. J.; Dingledine, R. Glutamate receptor ion channels: structure, regulation, and function. *Pharmacol. Rev.* **2010**, *62*, 405−496.

(2) Paoletti, P.; Bellone, C.; Zhou, Q. NMDA receptor subunit diversity: impact on receptor properties, synaptic plasticity and disease. *Nat. Rev. Neurosci.* **2013**, *14*, 383−400.

(3) Williams, K.; Russell, S. L.; Shen, Y. M.; Molinoff, P. B. Developmental switch in the expression of NMDA receptors occurs in vivo and in vitro. *Neuron* **1993**, *10*, 267−278.

(4) Costa, R. O.; Lacor, P. N.; Ferreira, I. L.; Resende, R.; Auberson, Y. P.; Klein, W. L.; Oliveira, C. R.; Rego, A. C.; Pereira, C. M. Endoplasmic reticulum stress occurs downstream of GluN2B subunit of N-methyl-d-aspartate receptor in mature hippocampal cultures treated with amyloid-beta oligomers. *Aging Cell* **2012**, *11*, 823−833.

(5) Mullasseril, P.; Hansen, K. B.; Vance, K. M.; Ogden, K. K.; Yuan, H.; Kurtkaya, N. L.; Santangelo, R.; Orr, A. G.; Le, P.; Vellano, K. M.; Liotta, D. C.; Traynelis, S. F. A subunit-selective potentiator of NR2C- and NR2D-containing NMDA receptors. *Nat. Commun.* **2010**, *1*, 90.

(6) Khatri, A.; Burger, P. B.; Swanger, S. A.; Hansen, K. B.; Zimmerman, S.; Karakas, E.; Liotta, D. C.; Furukawa, H.; Snyder, J. P.; Traynelis, S. F. Structural determinants and mechanism of action of a GluN2C-selective NMDA receptor positive allosteric modulator. *Mol. Pharmacol.* **2014**, *86*, 548−560.

(7) Krystal, J. H.; Karper, L. P.; Seibyl, J. P.; Freeman, G. K.; Delaney, R.; Bremner, J. D.; Heninger, G. R.; Bowers, M. B., Jr.; Charney, D. S. Subanesthetic effects of the noncompetitive NMDA antagonist, ketamine, in humans. Psychotomimetic, perceptual, cognitive, and neuroendocrine responses. *Arch. Gen. Psychiatry* **1994**, *51*, 199−214.

(8) Belforte, J. E.; Zsiros, V.; Sklar, E. R.; Jiang, Z.; Yu, G.; Li, Y.; Quinlan, E. M.; Nakazawa, K. Postnatal NMDA receptor ablation in corticolimbic interneurons confers schizophrenia-like phenotypes. *Nat. Neurosci.* **2010**, *13*, 76−83.

(9) Volgraf, M.; Sellers, B. D.; Jiang, Y.; Wu, G.; Ly, C. Q.; Villemure, E.; Pastor, R. M.; Yuen, P.-W.; Lu, A.; Luo, X.; Liu, M.; Zhang, S.; Sun, L.; Fu, Y.; Lupardus, P. J.; Wallweber, H. J. A.; Liederer, B. M.; Deshmukh, G.; Plise, E.; Tay, S.; Reynen, P.; Herrington, J.; Gustafson, A.; Liu, Y.; Dirksen, A.; Dietz, M. G. A.; Liu, Y.; Wang, T.-M.; Hanson, J. E.; Hackos, D.; Scearce-Levie, K.; Schwarz, J. B. Discovery of GluN2A-Selective NMDA Receptor Positive Allosteric Modulators (PAMs): Tuning Deactivation Kinetics via Structure-Based Design. *J. Med. Chem.* **2016**, *59*, 2760−2779.

(10) Rogawski, M. A. AMPA receptors as a molecular target in epilepsy therapy. *Acta. Neurol. Scand.* **2013**, *127*, 9−18.

(11) Hawkins, P. C. D.; Skillman, A. G.; Nicholls, A. Comparison of Shape-Matching and Docking as Virtual Screening Tools. *J. Med. Chem.* **2007**, *50*, 74−82.

(12) ROCS 3.2.1.4: OpenEye Scientific Software, Santa Fe, NM. http://www.eyesopen.com.

DOI: 10.1021/acsmedchemlett.6b00388
ACS Med. Chem. Lett. 2017, 8, 84−89

(13) eMolecules, Inc., La Jolla, CA. http://www.emolecules.com.
(14) Feng, J. A.; Aliagas, I.; Bergeron, P.; Blaney, J. M.; Bradley, E. K.; Koehler, M. F. T.; Lee, M. L.; Ortwine, D. F.; Tsui, V.; Wu, J.; Gobbi, A. An integrated suite of modeling tools that empower scientists in structure- and property-based drug design. *J. Comput.-Aided Mol. Des.* **2015**, *29*, 511−523.
(15) Burger, A. Isosterism and bioisosterism in drug design. *Prog. Drug Res.* **1991**, *37*, 288−362.
(16) Wager, T. T.; Hou, X.; Verhoest, P. R.; Villalobos, A. Moving beyond Rules: The Development of a Central Nervous System Multiparameter Optimization (CNS MPO) Approach To Enable Alignment of Druglike Properties. *ACS Chem. Neurosci.* **2010**, *1*, 435−449.
(17) Hackos, D. H.; Hanson, J. E. Diverse modes of NMDA receptor positive allosteric modulation: Mechanisms and consequences. *Neuropharmacology* **2016**, *112*, 34−45.
(18) Hackos, D. H.; Lupardus, P. J.; Grand, T.; Chen, Y.; Wang, T.-M.; Reynen, P.; Gustafson, A.; Wallweber, H. J. A.; Volgraf, M.; Sellers, B. D.; Schwarz, J. B.; Paoletti, P.; Sheng, M.; Zhou, Q.; Hanson, J. E. Positive allosteric modulators of GluN2A-containing NMDARs with distinct modes of action and impacts on circuit function. *Neuron* **2016**, *89*, 983−999.

DOI: 10.1021/acsmedchemlett.6b00388
ACS Med. Chem. Lett. 2017, 8, 84−89